



POLITECNICO
MILANO 1863

SCUOLA DI INGEGNERIA INDUSTRIALE
E DELL'INFORMAZIONE



EXECUTIVE SUMMARY

Molecular Excitons in Dielectric Metasurfaces

MASTER OF SCIENCE IN MATERIALS ENGINEERING AND NANOTECHNOLOGY -
INGEGNERIA DEI MATERIALI E DELLE NANOTECNOLOGIE

Author: MARCO MARANGI

Supervisor: GUGLIELMO LANZANI

Co-supervisor: CESARE SOCI

Academic year: 2021-2022

1. Introduction

This thesis investigates the interaction between light and matter in coupled dielectric metasurfaces and molecular aggregates thin films. It explores the opportunities of developing hybrid systems that allow to tune the radiative properties of molecular excitons operating in the visible, with the potential of working at room temperature.

The aim of this work was to develop room-temperature polaritonic devices that can achieve both weak and strong coupling in the visible range by designing a variety of metasurface designs and fine-tuning the optical properties of the emissive material through supramolecular chemistry. For this proof of principle demonstration, for the dielectric metasurface we have chosen a TiO₂ thin film, while for the emissive counterpart we have chosen the J-aggregate formed by aggregating the TDBC cyanine dye. Due to the coupling between the two components, the isotropic excitonic emission is imparted with directional emission according to the geometrical features of the dielectric metasurface.

Novel insights into the design and possible applications of coupled dielectric metasurface molec-

ular aggregates through both simulated and experimental results will be presented throughout this work, setting the foundations for further developments of superradiant devices based on J-aggregates.

2. Theoretical Background

2.1. Dielectric Optical Resonators^[6]

In recent years, the study of light-matter interactions has garnered a great deal of attention from researchers due to the potential to control light confinement at the nanoscale. Advances in nanofabrication have made it possible to design and fabricate subwavelength nanostructured materials that can control and enhance the electromagnetic field distribution of light in a variety of ways.

This concept is based on the principle of light scattering with structures of size comparable to the incoming wavelength, which according to Mie theory causes strong scattering resonances both in metallic and dielectric structures. In its simplest form, Mie theory predicts that the scattering phenomena associated with a material will depend on its permittivity and a size parameter defined by the geometry of the ob-

ject. The response of a metallic material differs from that of a dielectric material because their permittivity is opposite in sign.

The interaction between light and a metallic nanoparticle whose size is comparable to that of the incoming radiation causes an electric response from the particle that can be associated with the emergence of a localized surface plasmon resonance. While the interaction with a dielectric nanoparticle can generally cause both an electric and magnetic response depending on the specific displacement currents generated in the material.

Plasmonic resonators have long been employed in nanophotonics due to their capability to efficiently confine the electromagnetic field to small volumes and thus have strong local field enhancements. However, these materials are heavily limited by their considerable Ohmic losses, particularly in the visible range.

High refractive index dielectric materials have generated a great deal of interest in the last decade due to their high real refractive index and low dissipative losses. Multiple studies have shown how these materials can lead to high quality factor nanostructures that work for a variety of resonances.

The type of response and its strength strongly depend on the refractive index of the material and, to some extent, the surrounding volume. It is also heavily affected by the specific geometry of the object; modifying the geometrical features of the resonator will inevitably alter the relative spectral position of the resonances involved, as well as its optical character.

Considering all the advantages of dielectric materials, we have chosen TiO_2 thin films to be nanostructured into dielectric metasurfaces that will serve as a substrate to the molecular aggregate thin film.

Metasurfaces ^[1, 4] The periodic repetition in space of a planar pattern of resonators of sub-wavelength thicknesses is known as a metasurface. In these structures, the optical response of the bulk pattern will differ from that of the single resonator, hence the design criteria between the two will differ even though all that has been mentioned above regarding size and permittivity still holds true. The base concept of light interacting with a resonator also remains present in

metasurfaces, but the presence of multiple objects that interact with the same incoming radiation allows for more freedom in the design process and plenty of possible applications.

The design flexibility of metasurfaces allows us to accomplish impressive feats such as wavefront shaping, nearly perfect absorption, reflection or transmission, induced polarization, and chirality, along with many more applications. However, working with a large number of resonators, designing for a specific resonance wavelength becomes a sensitive task due to the potential impact of fabrication tolerances and error propagation. Despite recent advances in fabrication techniques that have reduced the presence of such artifacts, the complexity of the fabrication process inevitably increases when moving to visible wavelengths because of the reduced size of the resonators.

While it is possible to design a metasurface to be less sensitive to fabrication tolerances, achieving high-quality factor cavities in the visible spectrum remains a relatively new and challenging field, hence further advances in nanofabrication techniques must be developed for fabricated metasurfaces to be reliable substrates for more complex fully integrated devices. Regardless of such challenges, thanks to careful design and refined fabrication processes, we have been able to fabricate dielectric metasurfaces able to efficiently couple with molecular aggregates thin films in the visible range.

2.2. Molecular Excitons^[3, 7]

J-aggregates are a class of molecular aggregates consisting of highly ordered molecular assemblies of dyes or other chromophores. In these aggregates, the units are arranged in a one-dimensional chainlike structure that allows for strong electronic coupling between the sub-units, resulting in unique optical properties. The J-band peak, which is red-shifted from the monomeric peak, emerges from the excitonic coupling between the units in the aggregate. This results in a delocalized excitonic state of great intensity (Figure 1), which distinguishes these structures from other emissive materials.

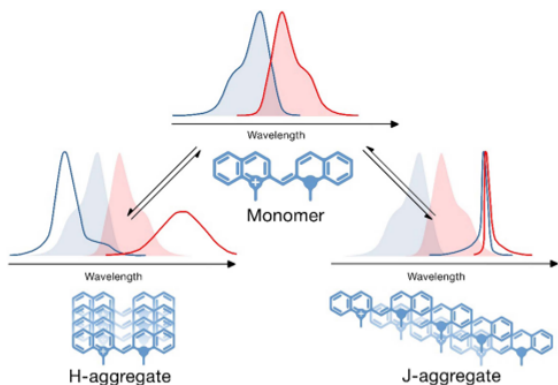


Figure 1: Schematic representation of the spectral changes following the formation of H- and J- aggregates in cyanine dyes [5].

The ordered self-assembled structure of J-aggregates allows for the formation of delocalized excitonic states spanning over multiple sub-units, leading to an increase in the rate of emission of the aggregates. This phenomenon is an extension of the concept of "superradiance," introduced by R. H. Dicke in 1953. J-aggregates can be formed by a wide range of dyes and chromophores, and the formation of J-aggregates is influenced by a number of factors, including the structure of the chromophore, the solvent polarity, and the aggregation conditions.

J-aggregates have many potential applications in sensing, imaging, and optoelectronics. They have been used as fluorescent probes for biomolecules and cells, as well as for the detection of environmental pollutants. They have also been incorporated into organic solar cells and light-emitting diodes, where their unique optical properties can improve device performance. Researchers are actively exploring ways to control the formation and morphology of J-aggregates in order to be able to exploit their unique optical properties in more complex systems in tandem with other materials.

Superradiance R.H. Dicke introduced the concept of superradiance in 1954 [2], suggesting that molecules interacting within a shared radiation field cannot be considered independent oscillators and their radiative behavior will be influenced by their degree of coherence. The dipole moment of the ensemble of radiating objects is given by the sum of the expectation values of each dipole moment. Additionally, such systems will radiate coherently in the direction

of excitation, since all the other components will interact to cause transitions to states of lower cooperation number. In the past few decades, research has confirmed the validity of Dicke's model and developed more advanced theoretical frameworks.

Experimental observation of superradiance is challenging because of local disorder, inhomogeneous broadening, and temperature-related phenomena that cause dephasing between oscillating dipoles and a reduction of coherence within the system. However, claims of superradiant behavior have been reported in literature in materials such as H-Aggregates, quantum dots, and perovskites thin films. Theoretical models predict that a superradiant system will show an increase in the decay rate of emission, a burst in the cavity mode population, and a non-linear dependence of the maximum of photoluminescence from the number of coupled emitters.

Experimentally, non-linearity of emission in pump fluence measurements and photon bunching are typical of strongly coupled systems of quantum emitters. Achieving superradiance experimentally and being able to foster its emergence at room temperature is a field of great interest for researchers due to the possibility of exploiting it to create ultrafast, highly selective, and directional emitters for applications in a variety of fields such as bioimaging and multi-photon high-brightness quantum light sources, as well as in fields on the rise such as optical and quantum computing.

3. Numerical Simulation Methods

The simulated results presented in this work have been calculated through the commercial softwares Ansys Lumerical Finite-Difference Time-Domain and Comsol Multiphysics. The device configuration that has been simulated consists of a 1 mm quartz substrate, followed by a 200 nm film of patterned TiO₂ which is then completely covered by a TDBC thin film as the J-aggregate based emissive material. A wide array of simulated results including transmittance spectra as a function of geometrical sweeps, electric field distributions, and angle-resolved transmittance spectra will be presented and discussed in the next paragraphs.

The principles behind the design process em-

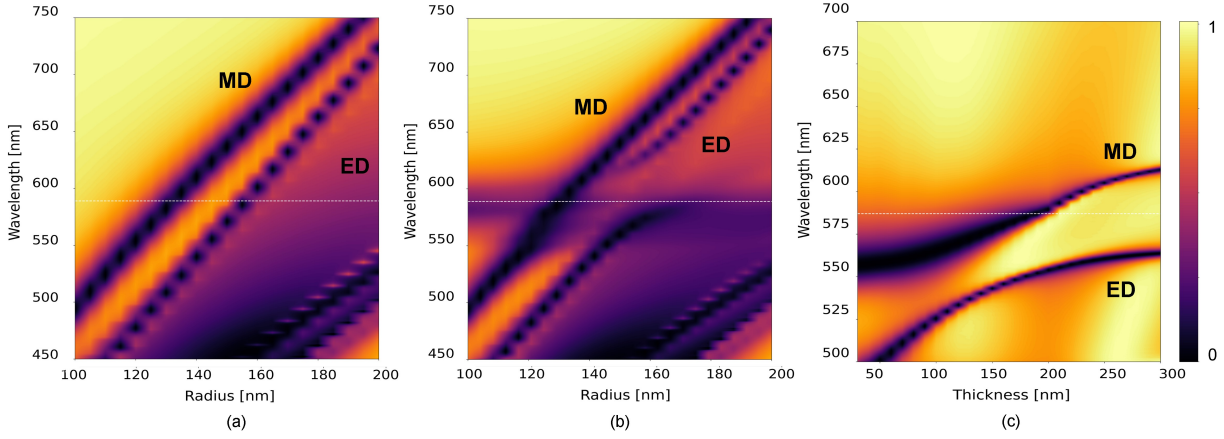


Figure 2: a,b) Normal-incidence transmission spectra of cylinders of multiple radii in the form of a 2D colourmap for the bare (a) and active (b) structure. c) Normal-incidence transmission spectra as a function of the thickness of the TDBC thin film for the passive structure.

ployed in this work were to provide a variety of metasurfaces working at distinct optical resonances and quality factors so that different coupling regimes between the metasurface and the molecular aggregates could be investigated.

Since the dimensions of the resonators are comparable to the wavelength of the incoming excitation, the optical resonances of the metasurfaces will be strongly dependent on the size and geometrical features of the resonators. Consequently, finding the right set of geometrical parameters associated to each distinct resonance requires precise investigation of how each parameter affects the optical behaviour. This concept will be studied by performing parameter sweeps, large batches of simulations where one geometrical parameter is varied within a range, while all other parameters are kept constant.

Two major classes of optical resonances will be presented in this manuscript: the Mie and the quasi-bound states in the continuum resonances.

3.1. Mie Resonances

Three types of structures will be discussed in the following paragraphs:

- The **bare metasurface**: patterned TiO_2 on a glass substrate.
- The **passive structure**: the bare metasurface surrounded by the molecular aggregate thin film with a constant refractive index (\mathbf{n}) corresponding to the value of \mathbf{n} at high wavelengths.
- The **active structure**: the bare metasurface surrounded by the molecular aggregate

gate thin film as an absorbing material with its refractive index depending on the wavelength.

The bare metasurface will be used to identify the resonance and fine tune the geometrical parameters. The passive structure will instead be important to estimate how introducing another high-index material influences the resonance and in particular the near-field electromagnetic field distribution (or mode volume). The active structure is analysed to estimate the extent of coupling between the photonic resonators and the excitonic active material, eventually exposing the presence of polaritons under the right conditions.

Parameter Sweeps Knowing that the magnetic dipole resonance can be generated when the wavelength of light within the dielectric resonator is comparable to the particle's diameter $D = \lambda/n$ the preliminary dimensions of the resonators can be roughly estimated. Fine tuning of the size and spacing of the resonators within the unit cell will then be required to achieve stronger light-matter interactions and resonances with a stronger electric or magnetic dipole character.

The resonance can be initially identified by a pronounced dip in transmittance, associated with a strong interaction between light and matter, meaning that the electromagnetic field of the incoming radiation has been localized within the patterned dielectric and redistributed throughout space depending on the specific geometry and the surrounding refractive index.

Figure 2 (a) represents the normal-incidence radius-sweep plot for the bare structure, two bands can be distinguished by a dip in transmittance that shifts along with the radius. The higher wavelength band can be attributed to the magnetic dipole resonance (MD), while the lower wavelength band can be identified as the electric dipole resonance (ED). An increase in volume of the resonators, shown in this figure by higher radii ($R > 150 \text{ nm}$), allows the multipole resonances to arise at lower wavelengths.

This batch of simulations allowed us to determine the magnetic (MD) and electric dipole (ED) resonances for the bare metasurfaces without active dissipative TDBC thin film.

The same simulation setup was used to investigate the optical response of the two resonances when the molecular aggregate thin film behaves as an active dissipative material (Figure 2 (b)), hence with both real and imaginary permittivity expressed as a function of wavelength. Here, both bands split into two distinct peaks each for the radii associated to the on-resonance configurations (MD and ED). These additional peaks, which were not found in the original bare structure, can be attributed to the formation of exciton-polaritons in the weak-coupling regime. Additionally, Figure 2 (c) shows how the optical response of the metasurface is affected by a passive TDBC film of varying thickness. The electric field distribution of the MD and ED configurations did not change with the presence of films of different thickness, thus the two Mie resonances can be deemed robust under the presence of the molecular aggregate thin film.

A more refined discussion of the design process, supported by a variety of parameter sweeps, can be found in the complete manuscript.

Angle-resoled Transmittance Angle-resolved transmittance measurements can be used to study the dispersion of exciton-polaritons, as further proof of their manifestation in a hybrid photonic device. The exciton-polariton optical signature can be associated to dips in transmittance after light passes through the metasurface covered by the active molecular aggregate thin film. Angle-resolved transmittance spectra will also display the exciton-polaritons dispersion, allowing us to distinguish them from other optical resonances.

The lower polariton dispersion bands have been highlighted by the white dashed lines and labeled LP. The associated energy splitting for the MD resonance is $E_{splitting} \approx 318 \text{ meV}$, while for the ED resonance is $E_{splitting} \approx 400 \text{ meV}$.

3.2. Quasi-Bound States in the Continuum

The unit cell and the field distribution of the ED Q-BIC is shown in Figure 4.

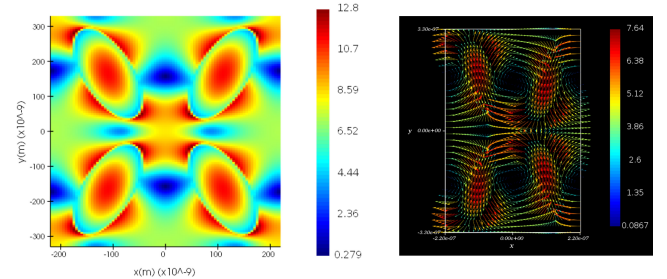


Figure 4: Electric field distribution for the ED quasi-bound state in the continuum resonance. The latter univocally identifies the optical resonance.

The angle-resolved transmittance spectra for this resonance are shown in the last column of Figure 3. In this case, the energy splitting for the polaritons is $E_{splitting} \approx 370 \text{ meV}$.

4. Sample Fabrication

The devices fabricated in this work are composed of a multilayer structure (Figure 5), consisting of three different materials stacked on top of each other. The bottom layer is a 1 mm thick quartz substrate. The middle layer is a 200 nm thick TiO_2 metasurface. The top layer is a thin film of TDBC J-aggregate (Figure 8 (a)).

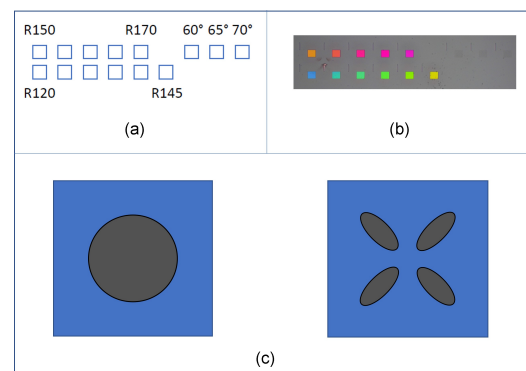


Figure 5: a) Schematic representation of the fabricated arrays. b) Optical micrograph of the fabricated arrays. c) Schematic representation of the unit cell of the ED-MD Mie and ED Q-BIC optical resonances.

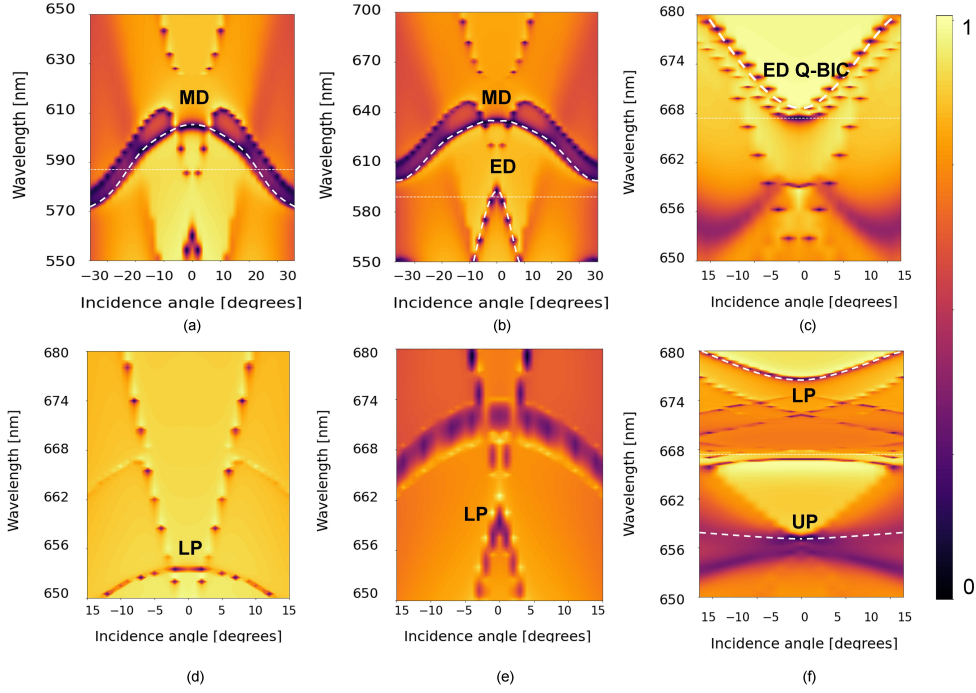


Figure 3: Simulated angle-resolved transmission spectra for the MD $R = 120$ nm (a), ED $R = 130$ nm (b), and Q-BIC (c) resonances covered by the TDBC film in its passive form. d-f) Simulated angle-resolved transmission spectra for the active structure of the same resonances showing the emergence of the lower polariton bands.

The fabrication process consists of five steps: in solution growth of the molecular aggregate, sputtering of TiO_2 on quartz, electron beam lithography (EBL) of TiO_2 , dry etching to transfer the metasurface pattern, and spincoating of TDBC on the metasurface.

Sputtering of TiO_2 The first step in the fabrication of metasurfaces is the deposition of 200 nm TiO_2 thin films on top of a 1 mm thick quartz substrate. The latter is cleaned beforehand by sonication in water, acetone, and isopropanol for 5 minutes per step.

The TiO_2 thin film is deposited by sputtering at a vacuum pressure of roughly 10^{-7} mbar in a Ar atmosphere and a power of 150 W with deposition rates ranging from 1.75 to 2.35 $\frac{\text{nm}}{\text{min}}$ depending on the physical position of the substrates with respect to the 99.99% titanium dioxide target.

Electron Beam Lithography The EBL and dry etching steps have undergone a series of attempts with varying degrees of success. The most successful attempt will be discussed in this paragraph and the next.

In this case, a 30 nm chromium hard mask was

deposited on top of the 200 nm titanium dioxide film to serve as a protective layer during the etching step. A 120 nm HSQ thin film was spin coated at 5000 rpm for 60 seconds, followed by a softbake step at 140°C for 3 minutes. The sample was then exposed through EBL at dosages varying between 0.9 and 1.2 $\frac{\mu\text{s}}{\text{dot}}$, with the best results later found to be associated to the 1.1 and 1.2 $\frac{\mu\text{s}}{\text{dot}}$ dosages. The exposed sample was immersed in a salty developer (1 wt.% NaOH and 4 wt.% NaCl in deionized water) for 4 minutes, followed by a rinse in deionized water.

The fabricated structures appeared to be more uniform in size and spatial distribution, with overall fewer defects (Figure 7).

Dry Etching Following development, the HSQ layer will have been patterned according to what has been written during EBL, hence the chromium hard mask underneath can now be selectively etched to expose the TiO_2 bottom layer. The chromium thin film is etched using inductively-coupled plasma reactive ion etching (ICP-RIE) with a mixture of Cl_2 and O_2 .

The TiO_2 can now be selectively etched with CHF_3 gas. During this process the top HSQ layer will gradually etch eventually exposing the Cr hard mask underneath. The latter will act as

a protective layer since its etching rate in CHF_3 is much lower than that of TiO_2 . Depending on the thickness of the TiO_2 layer, a thin chromium film could be left over on top of the now patterned TiO_2 . Being a dissipative material by nature, it is important that the residual chromium is removed so as not to worsen the optical properties of the device. To do so, the sample was immersed in a commercially available chromium liquid etchant for a few minutes. The sample is then rinsed in deionized water and IPA, and then dried with N_2 .

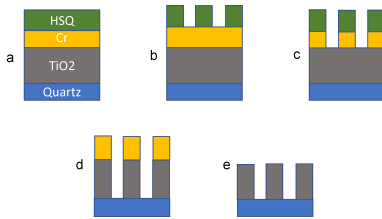


Figure 6: Schematic representation of the fabrication process using a chromium hard mask. a) Unpatterned sample. b) EBL exposure and development of HSQ resist. c) ICP-RIE of Cr hard mask. d) CHF_3 RIE of TiO_2 . e) Cr wet etching.

Figures 7 (a) and (b) show the metasurfaces throughout the improved fabrication process for respectively the MD and ED Mie and ED Q-BIC resonances.

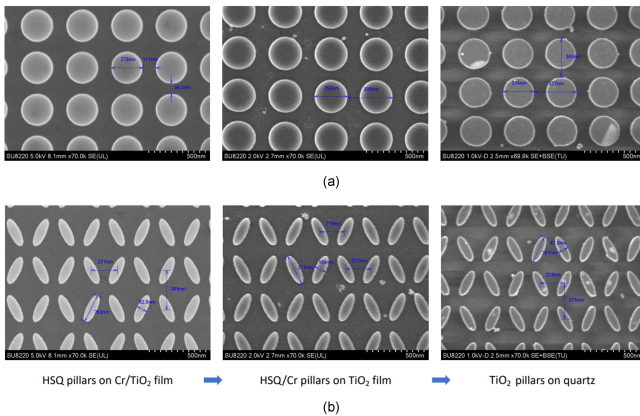


Figure 7: a) SEM images of the cylinders-based (Mie) and elipsoidal-based (Q-BIC) metasurfaces throughout the fabrication process.

Synthesis of the TDBC J-aggregate The TDBC monomer was dissolved in DI water at a concentration of $2.5 \frac{\text{mg}}{\text{mL}}$ and left to aggregate for 24 hours at room temperature, covered from light exposure. A solution of $64 \frac{\text{mg}}{\text{mL}}$ of Poly(vinyl alcohol) was prepared by further polymerizing

PVA in DI water for 4 hours at 90°C under constant stirring.

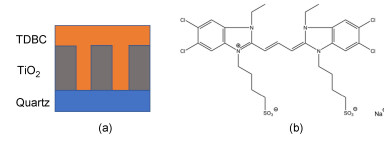


Figure 8: a) Side view of the schematic representation of the fully integrated device. b) Structural formula of 5,6-Dichloro-2-[[5,6-dichloro-1-ethyl-3-(4-sulfobutyl)-benzimidazol-2-ylidene]-propenyl]-1-ethyl-3-(4-sulfobutyl)-benzimidazolium hydroxide, inner salt, sodium salt in its monomeric form.

The grown TDBC molecular aggregate and the PVA solution were then mixed in a 1:1 ratio. The addition of PVA is required to ensure better filmability by supplying a stable matrix to the aggregate.

Spincoating of TDBC A volume of $100 \mu\text{L}$ of the mixed TDBC-PVA solution is spincoated at 2000 rpm for 60 seconds on top of the patterned metasurfaces. The film is then further dried at 4000 rpm for 30 seconds.

5. Experimental results

5.1. Normal-incidence Transmittance

The bare fabricated metasurfaces have been characterized by normal-incidence transmittance measurements to confirm the success of fabrication by comparing the spectra of the various arrays with the simulated results.

The normal-incidence spectra of the arrays associated with the MD and ED resonances of the sample that will be referred to as S1 from now on can be seen on the left and right of Figure 9 respectively.

The MD resonance (Figure 9 left panel) seems to precisely match the simulated results. While the ED resonance (Figure 9 right panel) is slightly blue shifted with respect to the simulated results due to fabrication tolerances, which means that the resonance that matches the experimental results is associated to the array of radius $R = 155 \text{ nm}$).

In both cases, the overall lower values of transmittance can be attributed to inevitable fabrication tolerances and intrinsic Ohmic losses of the TiO_2 thin film. This should not pose an issue since the presence of the TDBC thin film will

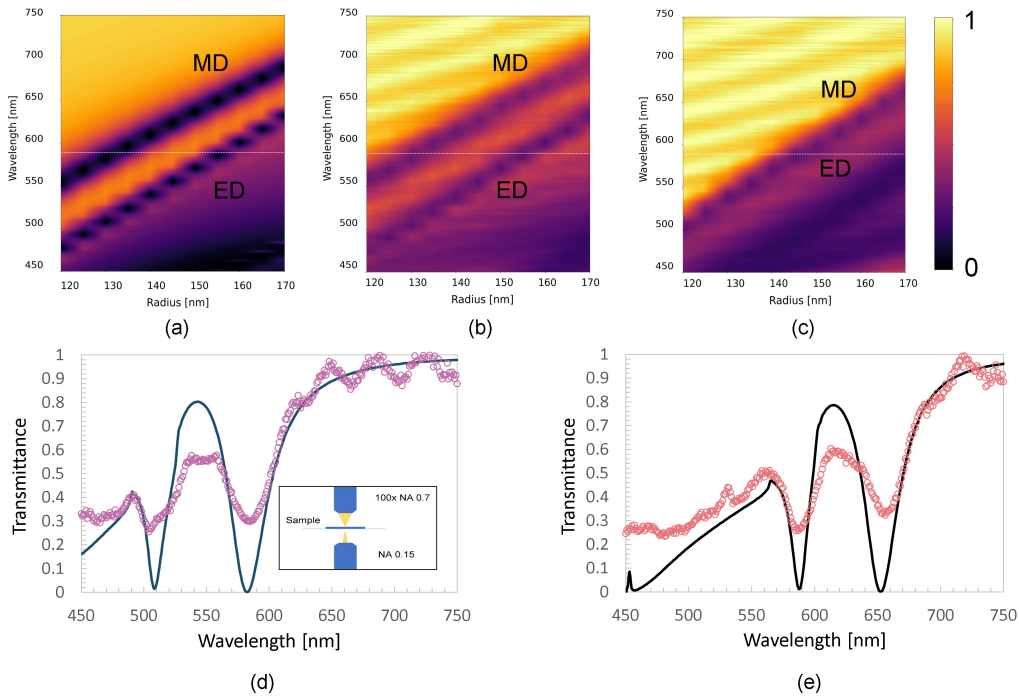


Figure 9: Comparison between the simulated (a) and simulated (b,c) normal-incidence transmittance for unit cells of different radii for sample S1 (b) and S2 (c). The MD and ED bands are shown to perfectly match between the experimental and calculated results for sample S1 attributed to figure (b), while the response is blueshifted for S2 suggesting overetching. d,f) Experimental (dotted) and simulated (continuous line) transmittance spectra of the magnetic dipole (left) and electric dipole (right) Mie resonances. The inset shows the simplified schematics of the optical setup used to measure the transmittance.

increase the resonance strength due to its high refractive index, as shown for the passive structure in the chapter on simulations and as will also be shown by the angle-resolved photoluminescence measurements in this chapter.

These measurements have been repeated for all arrays, allowing us to evaluate the quality of fabrication for each dosage and sample. Figure 9 (b,c) shows the normal-incidence transmittance spectrum for the radius sweep associated to the highest dosage, these results can be compared to the simulated spectra present in the same figure (a). The match between the experimental results for this sample can be considered as excellent, hence these metasurfaces can be used as substrates for the TDBC thin-film deposition step.

5.2. Photoluminescence as a Function of Pumping Power

The optical properties of J-aggregates have been shown to be influenced by the pumping power used to excite their emission. The reason being that the ordered chains of unit molecules found in aggregates are able to couple with each other

and radiate coherently, meaning that the resulting emission will be dependent on the number of units that are coupled and thus on the pumping power they are subjected to. This phenomenon can be quantified by measuring the response of the aggregates to different excitation powers.

To highlight this characteristic property of J-aggregates, a series of normal-incidence photoluminescence measurements were performed on a TDBC:PVA thin film on a 1 mm quartz substrate. The film was excited by a pulsed laser at an excitation wavelength of 405 nm with a repetition rate of 80 MHz over a range of roughly 10 – 90 μW of excitation power with a 100x objective.

A closer look at the data in Figure 10 shows that the optical response of the aggregate can be divided into two regions by a pumping power threshold of roughly $P_{threshold} = 60 \mu W$. This behaviour is further highlighted in the double logarithmic plot in Figure 10. While data points before the threshold can be fit with the equation of a straight line, those after the threshold power are perfectly fit by the exponential function $f(x) = x^{4.884} \cdot 10^{-3.5927}$ meaning that

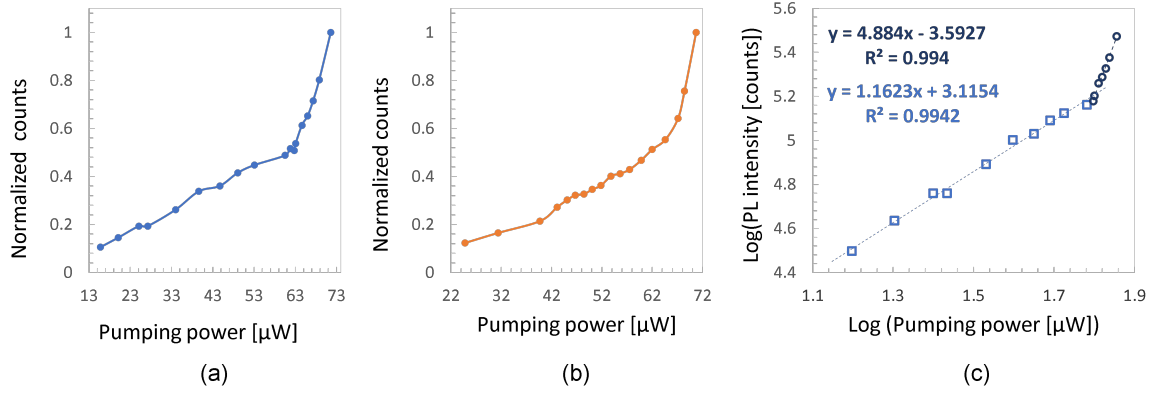


Figure 10: a,b) Normal-incidence photoluminescence measurements for sample A (a) and B (b). c) Double logarithmic plot of the normalized peak intensity of photoluminescence against the pumping power (sample A) showing a noticeable change in trend associated to cooperative emission.

the optical behavior of the aggregate has undergone a substantial change after what has been identified as the pumping threshold. This shift in response could be attributed to preliminary evidence of the emergence of cooperativity of emission associated with more coupled aggregate subunits induced by the increased pumping power. These results appeared to be reproducible with other similar samples.

5.3. Angle-resolved Photoluminescence Measurements

Angle-resolved photoluminescence (ARPL) measurements were performed for the final device in order to study the influence that the presence of a metasurface designed to work on-resonance with the emission wavelength of the (TDBC) thin film has on the emissive properties of the latter.

ARPL spectra were captured using an inverted optical microscope (Nikon Ti-U), a spectrograph (Acton IsoPlane SCT 320), and a charged-coupled detector (CCD, Andor iDus 420). A system of lenses was used to project the back focal plane of the collection objective (Nikon x50, $NA = 0.6$) into the slit of the spectrograph. The excitation wavelength has initially been set to 400 nm.

The ARPL spectrum for the resonators with $R = 130 \text{ nm}$ and $R = 155 \text{ nm}$, associated with the normal-incidence ED and higher angles ED Mie resonances are shown in Figure 11. The broad emission band without angle dependence centered at 590 nm is associated with the exciton of the TDBC thin film. The other bands

with a strong angle dependence can instead be attributed to the photonic bands of the metasurface. The structure is thus able to reach the weak coupling regime as shown by the optical bands being populated by photons at energies different from that of the pure excitonic state. The same measurements have been performed for the ED Q-BIC structure, as shown in Figure 12.

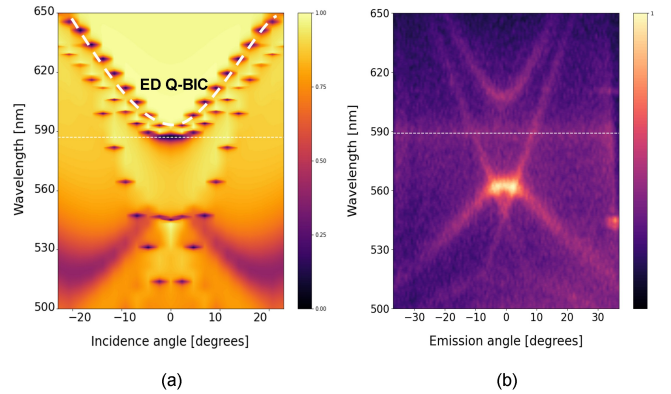


Figure 12: Simulated passive spectrum (a) and measured ARPL spectrum (b) for the symmetry protected electric dipole quasi-bound state in the continuum optical resonance.

All of these structures are able to couple with the exciton efficiently enough to show a sizeable difference in the directionality of emission of the J-aggregates. In fact, the angle-independent emission band of the exciton has now been imparted with an angle-dependent emissive behavior due to the available optical bands of the metasurfaces.

In this context, the photons associated with the incoming 400 nm radiation are localized within

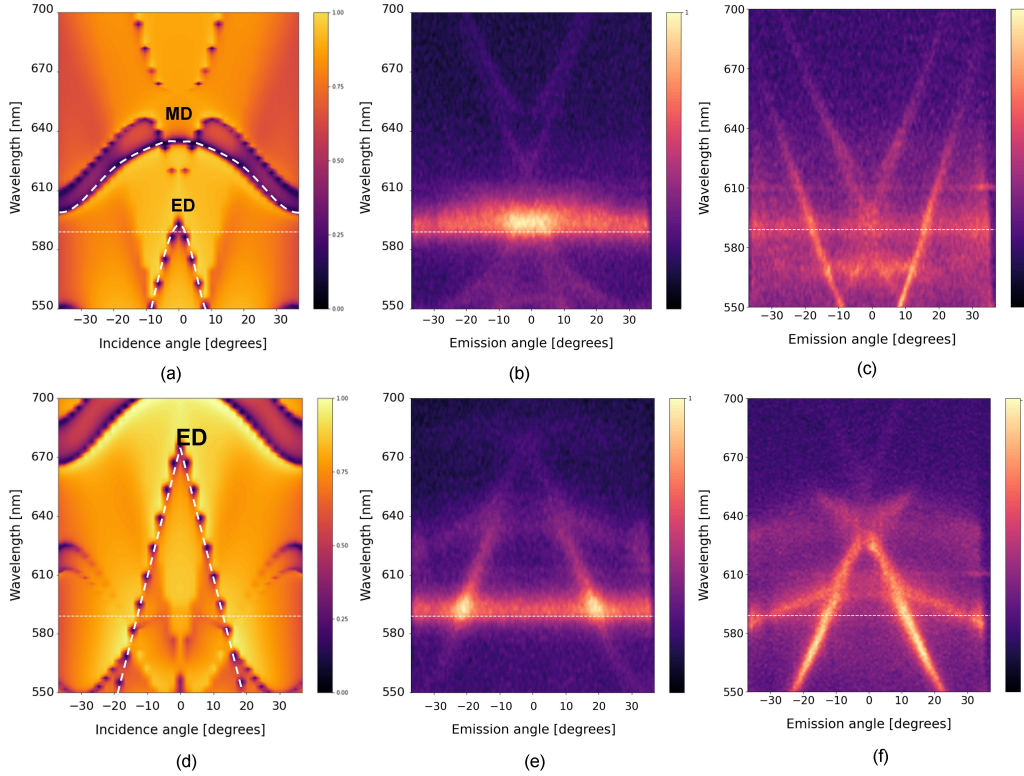


Figure 11: Simulated passive spectrum (a,d) and measured ARPL spectrum for the normal-incidence ED (b,c) and for the higher angles ED (d-f) resonances of two distinct samples (S1 in (b,e) and S3 in (c,f)) showing varying degrees of coupling between the J-aggregate thin film and the dielectric metasurface.

the TDBC thin film by the interaction with the resonators and are then able to excite the 589 nm emission from the J-aggregates. The newly emitted photons are then affected by the optical resonance of the metasurface and thus further localized within the TiO_2 resonators. This last step allows the emitted photons to be confined within the optical bands of the metasurface, leading to angle-dependent emission. More results related to the Q-BIC resonance can be found in the full manuscript.

6. Conclusions and Future Work

The aim of this thesis was to design dielectric metasurfaces with optical resonances that would overlap with the molecular exciton of J-aggregates so that the response of the latter could be investigated and could be tuned, in terms of its directionality and strength of emission. Additionally, this would serve as ground work to further push the limits of these unique hybrid systems to foster the emergence of super-radiance in J-aggregates.

The behavior of J-aggregates thin films coupled to dielectric metasurfaces operating under a variety of optical resonances in the visible spectrum and at room temperature has been investigated through both numerical and experimental work.

The fabricated metasurfaces were integrated with the tuned emissive J-aggregate thin film, so that the coupling between the two structures would allow us to study their interaction and the shift in optical response of the latter. To do so the band structure of the fully integrated device was first simulated and then investigated through angle-resolved photoluminescence measurements so that a direct comparison between simulated and experimental data could be made. This process allowed us to study the effects that different resonant cavities, working under distinct types of optical resonances, have on the emissive behaviour of J-aggregates.

These measurements showed that the two structures were able to couple efficiently and thus the incoming photons, localized by the metasurface, were able to strongly excite the molecular aggregate thin film and cause the newly emitted pho-

tions to populate the band structure of the metasurface, leading to a change in both wavelength and directionality of emission. The latter was shown to be highly tunable with changes in the geometry of the resonators, allowing us to control the generally angle-independent emission of J-aggregates to be directional.

Additionally, the decay rate of the excited states of J-aggregates is increased because of both the intrinsic properties of the aggregates and the Purcell effect induced by the metasurface working as an optical cavity. This phenomenon can be further enhanced by inducing superradiance in the J-aggregates, meaning that even faster devices could be theoretically fabricated. In this regard, the metasurface could foster room-temperature superradiance by localizing the electromagnetic field of the incoming excitation between the J-aggregates, leading to the development of ultrafast and high-directionality devices with a reduced power threshold for the emergence of superradiance.

This work bridges the gap between the field of molecular aggregates and metasurfaces, establishing foundational work to further develop hybrid devices capable of controlling the directionality and rate of emission. Being able to foster superradiance at room temperature would mean demonstrating the first evidence of non-isolated superradiant J-aggregates, thus allowing researchers to develop ultrafast and high-directionality emitters.

References

- [1] Antonio Ambrosio. Structuring visible light with dielectric metasurfaces. *Journal of Optics*, 20:113002, 10 2018.
- [2] R H Dicke, Palmer Physical, and I Aboratory. Coherence in spontaneous radiation processes. *Physical Review*, 93:99, 1 1954.
- [3] M Kasha, H R Rawls, and M Ashraf El-Bayoumi. The exciton model in molecular spectroscopy.
- [4] Kirill Koshelev, Sergey Lepeshov, Mingkai Liu, Andrey Bogdanov, and Yuri Kivshar. Asymmetric metasurfaces with high- q resonances governed by bound states in the continuum. *Physical Review Letters*, 121:193903, 11 2018.
- [5] Klaus Kreger, Hans-Werner Schmidt, Richard Hildner, Julia L Bricks, Yuri L Slominskii, Ihor D Panas, and Alexander P Demchenko. Fluorescent j-aggregates of cyanine dyes: basic research and applications review. *Methods and Applications in Fluorescence*, 6:012001, 12 2017.
- [6] Arseniy I. Kuznetsov, Andrey E. Miroshnichenko, Mark L. Brongersma, Yuri S. Kivshar, and Boris Luk'yanchuk. Optically resonant dielectric nanostructures. *Science*, 354, 11 2016.
- [7] Frank Würthner, Theo E. Kaiser, and Chantu R. Saha-Möller. J-aggregates: from serendipitous discovery to supramolecular engineering of functional dye materials. *Angewandte Chemie (International ed. in English)*, 50:3376–3410, 4 2011.